A general approach for MFe$_2$O$_4$ (M = Zn, Co, Ni) nanorods and their high performance as anode materials for lithium ion batteries

Nana Wang [a], Huayun Xu [a,*], Liang Chen [a], Xin Gu [a], Jian Yang [a], Yitai Qian [a,b]

[a] Key Laboratory of Colloid and Interface Chemistry, Ministry of Education and School of Chemistry and Chemical Engineering, Shandong University, Jinan 250100, PR China
[b] Hefei National Laboratory for Physical Science at Microscale and Department of Chemistry, University of Science and Technology of China, Hefei 230026, PR China

HIGHLIGHTS

- MFe$_2$O$_4$ (M = Zn, Co, Ni) nanorods have been synthesized using β-FeOOH as template.
- ZnFe$_2$O$_4$ exhibits a large capacity of 625 mAh g^{-1} at 1 A g^{-1} even after 300 cycles.
- CoFe$_2$O$_4$ and NiFe$_2$O$_4$ show 800 and 520 mAh g^{-1} respectively at 1 A g^{-1} over 300 cycles.

GRAPHICAL ABSTRACT
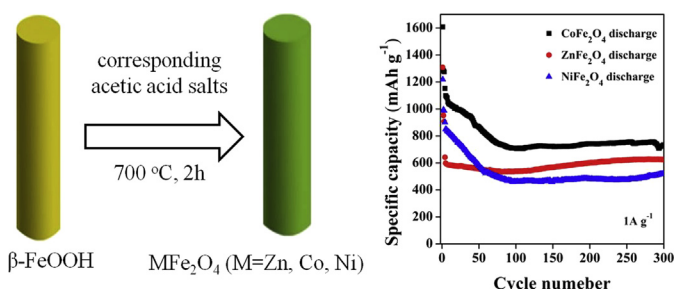
ARTICLE INFO

ABSTRACT

MFe$_2$O$_4$ (M = Zn, Co, Ni) nanorods are synthesized by a template-engaged reaction, with β-FeOOH nanorods as precursors which are prepared by a hydrothermal method. The final products are characterized by X-ray diffraction (XRD), scanning electron microscopy (SEM), and high-resolution transmission electron microscopy (HRTEM). The electrochemical properties of the MFe$_2$O$_4$ (M = Zn, Co, Ni) nanorods are tested as the anode materials for lithium ion batteries. The reversible capacities of 800, 625 and 520 mAh g^{-1} are obtained for CoFe$_2$O$_4$, ZnFe$_2$O$_4$ and NiFe$_2$O$_4$, respectively, at the high current density of 1000 mA g^{-1} even after 300 cycles. The superior lithium-storage performances of MFe$_2$O$_4$ (M = Zn, Co, Ni) nanorods can be attributed to the one-dimensional (1D) nanostructure, which can shorten the diffusion paths of lithium ions and relax the strain generated during electrochemical cycling. These results indicate that this method is an effective, simple and general way to prepare good electrochemical properties of 1D spinel Fe-based binary transition metal oxides. In addition, the impact of different reaction temperatures on the electrochemical properties of MFe$_2$O$_4$ nanorods is also investigated.

1. Introduction

Lithium ion batteries (LIBs) have attracted great attention and powered most of today's portable electronic devices due to their high energy density and long cycle life [1–4]. Graphite is widely used as anode material in commercial LIBs, owing to its low cost and long cycle life [2,3], but limited to a low theoretical capacity of 372 mAh g^{-1} which couldn't fulfill the demand for LIBs with high power and high energy density. Meanwhile, the possible reaction between lithiated graphite and the electrolyte is an inherent safety risk [3,5]. Therefore, further research is important to develop novel

anode materials combining suitable theoretical capacity and electrochemical stability. In this respect, transition metal oxides (e.g., MnO_2 [6], Fe_2O_3 [7], $ZnMn_2O_4$ [8]) have been thought as promising alternative anode materials due to their high specific capacity (600–1200 mAh g^{-1}) [9,10]. Unfortunately, their huge volume change during the discharge–charge process and poor electron (or Li-ion) conduction hindered their applications in LIBs [3,11–14]. Most recently, nanostructured materials have been proven to effectively contain the strain generated by volume change and give improved electron/Li-ion conduction [15,16]. Among various nanostructures, 1D nanomaterials are particularly attractive, owing to shortened Li-ion insertion/extraction distance, facile strain relaxation upon electrochemical cycling, and large surface to volume ratio, leading to improved electrochemical performances [6–8,13]. Therefore, 1D nanoscale transition metal oxides as anodes for LIBs are expected to give good electrochemical performance.

Fe-based materials stand out from the transition metal oxides due to their low cost and environmental benign [17]. Therefore, spinel Fe-based binary transition metal oxides with different morphologies have been synthesized through various methods to ameliorate the capabilities of LIBs. For example, $ZnFe_2O_4$ hollow spheres synthesized through a hydrothermal reaction and annealing process gave a specific capacity of about 900 mAh g^{-1} over 50 cycles [18]. $ZnFe_2O_4$ octahedrons obtained by one-step hydrothermal route showed a reversible capacity of 730 mAh g^{-1} after 300 cycles at the current density of 1000 mA g^{-1} [19]. $ZnFe_2O_4$ nanofibers were prepared through electrospinning technique (around 400 mAh g^{-1} at 800 mA g^{-1}) [20]. As for $CoFe_2O_4$ and $NiFe_2O_4$, cobalt and nickel spinel ferrites were prepared by a sol–gel process, with $CoFe_2O_4$ showing 740 mAh g^{-1} after 75 cycles and $NiFe_2O_4$ maintaining over 600 mAh g^{-1} after 80 cycles both at 1C [21]. Other structures such as macroporous $CoFe_2O_4$ [22], hollow $CoFe_2O_4$ nanospheres [23] and $NiFe_2O_4$ nanoparticles [24] were prepared, and their electrochemical properties were investigated. However, the electrochemical properties of 1D spinel Fe-based binary transition metal oxides were rarely systematically studied. Thus, developing a general and simple route to prepare 1D spinel ferrite nanostructure materials and systematically studying their electrochemical properties are essential.

In this work, MFe_2O_4 (M = Zn, Co, Ni) nanorods were synthesized by the calcinations of the as-obtained β-FeOOH nanorods with the corresponding metal acetates. Their electrochemical properties were investigated by galvanostatic discharge–charge and electrochemical impedance spectroscopy (EIS). The reversible capacities of 800, 625 and 520 mAh g^{-1} were obtained for $CoFe_2O_4$, $ZnFe_2O_4$ and $NiFe_2O_4$, respectively, at the high current density of 1000 mA g^{-1} even after 300 cycles. We also investigated the influence of reaction temperatures on the electrochemical properties of MFe_2O_4 nanorods to gain optimum performance.

2. Experimental section

2.1. Synthesis method

2.1.1. Synthesis of β-FeOOH nanorods

2 mmol of $FeCl_3 \cdot H_2O$ and 15 mmol of KNO_3 were dissolved in 40 mL of H_2O. Then, the solution was transferred into a stainless steel autoclave with a clean Teflon liner inside. After the autoclave was heated at 100 °C for 12 h, the product was collected by centrifugation and washed with water and ethanol several times. Finally, the yellow powders were dried at 60 °C for 6 h in air.

2.1.2. Synthesis of MFe_2O_4 nanorods

In a typical procedure, 2 mmol of the β-FeOOH powders and 1 mmol of metal acetates ($ZnC_4H_6O_4 \cdot 4H_2O$, $CoC_4H_6O_4 \cdot 4H_2O$ or

$NiC_4H_6O_4 \cdot 4H_2O$) were dispersed in 2 mL of acetone to generate a slurry. Then, the slurry was ball-milled for several hours and dried at 70 °C for 30 min in vacuum. The as-produced mixture was then calcined at 700 °C for 2 h in air. After cooled to the room temperature, the product was collected for the structure characterization and the electrochemical tests.

2.2. Characterization

The characteristics of the as-prepared samples were identified by X-ray powder diffraction (XRD, $Cu_{k\alpha}$ radiation, $\lambda = 1.5418$ Å). The materials were further characterized by transmission electron microscopy (TEM) using JEOL-1011 microscope, field-emission scanning electron microscopy (FESEM) with a JEOL JSM-7600F field emission instrument and high resolution transmission electron microscope (HRTEM, JEOL-2011) operating at 200 kV. Nitrogen sorption isotherm was examined on a Micromeritics ASAP-2000 instrument. Thermal gravimetric analysis (TGA) for the precursor was recorded on a Mettler Toledo TGA/SDTA851 thermal analyzer under air atmosphere.

2.3. Electrochemical measurements

The electrochemical performance of MFe_2O_4 (M = Zn, Co, Ni) nanorods were tested in a 2032-coin cell and characterized on Land-CT2001A battery cycler (Xinnuo, Wuhan, China) at room temperature. Working electrodes were prepared with the composition of MFe_2O_4:acetylene black:sodium carboxyl methyl cellulose (CMC) in the weight ratio of 60:30:10. The above mixture was milled (QM-3SP2 Planetary Ball Mill) for 5 h using H_2O as the solvent to form a homogenous slurry. Then the slurry was coated on Cu foil with a wet film thickness of 300 μm, and dried under vacuum at 80 °C for 12 h. The typical disk electrode contained active material of 2.2 mg cm^{-2}. The test cells were assembled in an argon filled glovebox (Mikrouna, Super 1220/750/900) with the separator of Celgard 2400 microporous membrane, lithium metal as an anode, and the electrolyte was a 1 mol L^{-1} solution of $LiPF_6$ dissolved in ethylene carbonate/dimethyl carbonate (EC/DMC) with a volume ratio of 1:1. The cyclic voltammograms (CVs) properties of $ZnFe_2O_4$ were tested by an LK-2005A electrochemical workstation (Lanlike, Tianjin China). Electrochemical impedance spectroscopy (EIS) was measured on an FRA-520 (MaterialsMates, Italia) connected to a Potentiostat-510 (MaterialsMates) over the frequency range of 100 kHz to 0.01 Hz.

3. Results and discussion

3.1. $ZnFe_2O_4$ nanorod

Fig. 1 shows the XRD patterns of the synthesized β-FeOOH and $ZnFe_2O_4$. All of the diffraction peaks in Fig. 1a can be indexed to tetragonal-phase β-FeOOH (JCPDS Card, No. 34-1266). After reacted with $ZnC_4H_6O_4 \cdot 2H_2O$ at 700 °C for 2 h in air, β-FeOOH transforms into $ZnFe_2O_4$ completely (JCPDS Card, No. 22-1012), as shown in Fig. 1b.

The morphologies of the β-FeOOH precursor and $ZnFe_2O_4$ were characterized by SEM and TEM images. As shown in Fig. 2a and b, the β-FeOOH obtained by a hydrothermal method presents as the short nanorods with their diameters of 60–80 nm and the length of 180–200 nm. After the high-temperature reaction at 700 °C, the resulting $ZnFe_2O_4$ preserves the one-dimensional shape and the similar sizes to those of β-FeOOH (Fig. 2a and b). This result agrees well with the template-engaged reaction [25]. The $ZnFe_2O_4$ nanorods were further characterized with HRTEM images. As shown in the inset of Fig. 2d, the lattice between neighboring fringes is
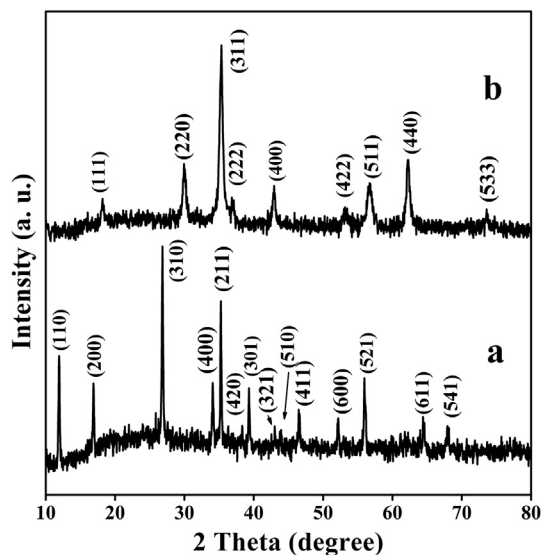
Fig. 1. XRD patterns of the as-prepared samples (a) β-FeOOH precursor and (b) ZnFe$_2$O$_4$ nanorods obtained at 700 °C.

Fig. 3. TGA curve of β-FeOOH and zinc acetate dihydrate.

0.467 nm which is consistent well with that of the (111) planes of ZnFe$_2$O$_4$.

The reaction process of β-FeOOH and ZnC$_4$H$_6$O$_4$·2H$_2$O was examined by TGA analysis (Fig. 3) with a heating rate of 10 °C min^{-1} in air. There are two apparent weight losses in the TGA curve. The first loss below 100 °C could be attributed to the removal of physically adsorbed water of ZnC$_4$H$_6$O$_4$·2H$_2$O. And the other one begins at 205 °C could be corresponded to β-FeOOH reacting with zinc acetate dihydrate and release of water and carbon oxides. Typically, we observed a weight loss of ∼8.2% for the first step and ∼31.1% for the second step (which agrees with the theoretical value of 33.2%). From the TGA curve, it can be seen that the ZnFe$_2$O$_4$ could be obtained at 359 °C. Mesoporous ZnFe$_2$O$_4$ nanorods with surface area of 22.987 m^2 g^{-1} were synthesized at 500 °C for 2 h (Figs. S1b
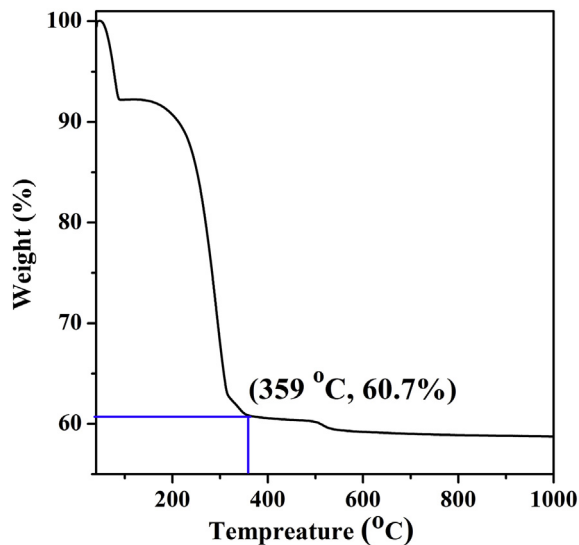
and S2a). While the ZnFe$_2$O$_4$ nanorods shows a relative smooth surface without pore-like structure when synthesized at 700 °C, which matches well with the BET result (surface area of 11.250 m^2 g^{-1}) (Fig. 2b, Fig. S2b). This difference may because that high temperature treatment could destroy pore-like structures [26]. It is believed that electrochemical properties possibly depend on the size, morphology and crystallinity of electrode materials [21,27–29], which will be discussed in the following paragraphs.

Firstly, cyclic voltammograms (CVs) of the electrodes made by ZnFe$_2$O$_4$ nanorods obtained at 700 °C were given in Fig. 4a. The broad peak centered at 0.55 V in the first cycle can be attributed to the reduction of Zn^{2+} and Fe^{3+} to Zn^0 and Fe^0, the formation of Li–Zn alloy and solid electrolyte interphase (decomposition of the electrolyte) [19,30,31]. In the subsequent cycles, the cathodic peak shifts to 0.92 V which may be related to a structure rearrangement
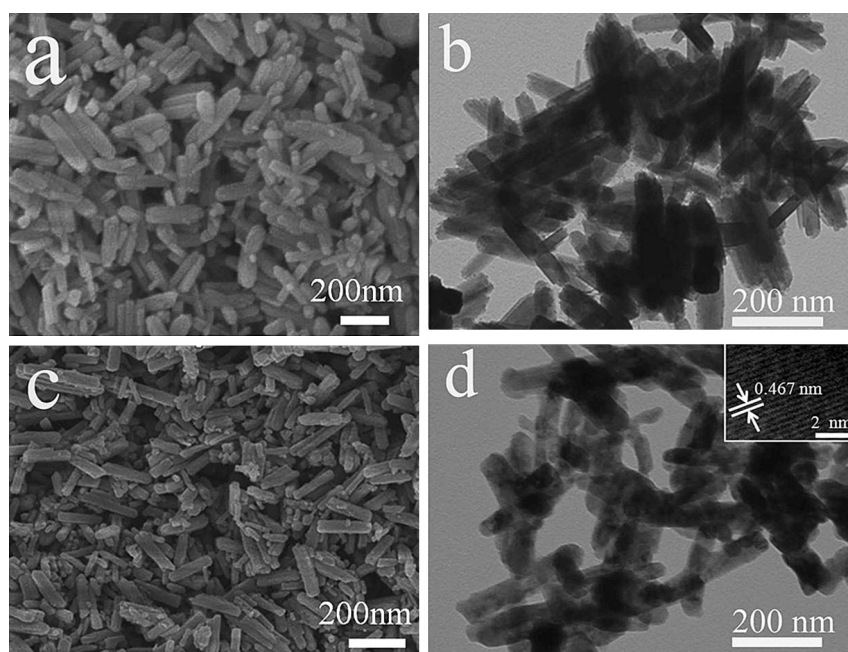

Fig. 2. SEM (a) and TEM (b) images of the β-FeOOH. SEM (c) and TEM (d) images of ZnFe$_2$O$_4$. Inset of (d) is the HRTEM image of ZnFe$_2$O$_4$.
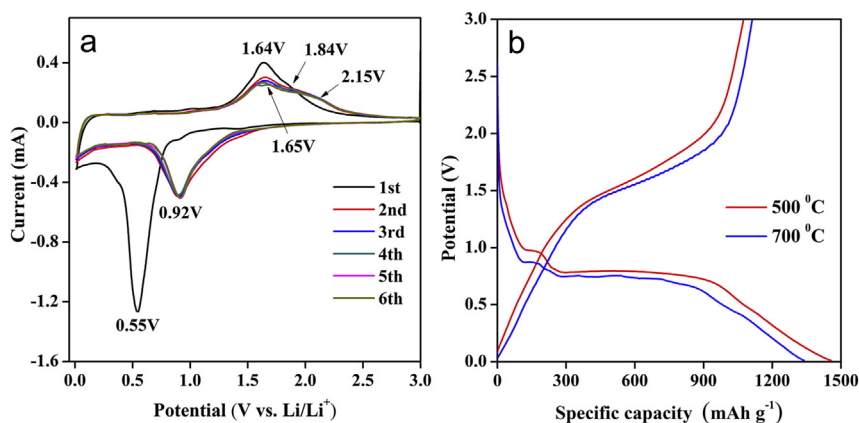
Fig. 4. (a) Cyclic voltammograms of the ZnFe$_2$O$_4$ sample obtained at 700 °C scanning at a rate of 0.1 mV s^{-1} in the voltage of 0.01–3.0 V vs. Li/Li$^+$ and (b) The initial charge–discharge profiles of the ZnFe$_2$O$_4$ nanorods obtained at 500 and 700 °C at a current density of 150 mA g^{-1} in the voltage range 0.01–3.0 V.

and associated with the reversible reduction of Fe^{3+} and Zn^{2+} [19,20,31]. During the anodic process, two peaks in the first cycle centered at 1.64 and 1.84 V can be attributed to the oxidation of Zn^0 and Fe^0 to ZnO and Fe$_2$O$_3$, respectively [19,31], which shift a bit in the subsequent cycles. The CV curves are well overlapped after the second cycle, indicating good electrochemical reversibility and capacity retention for ZnFe$_2$O$_4$ nanorods. Fig. 4b presents the initial charge–discharge profiles of ZnFe$_2$O$_4$ nanorods obtained at 500 °C and 700 °C within the potential range of 0.01–3 V at a current density of 150 mA g^{-1} (vs. Li/Li$^+$). For both samples, it can be observed that the initial discharge curve shows two apparent

plateau located at 0.9 V and 0.8 V, which can be attributed to the formation of Li$_x$ZnFe$_2$O$_4$ and the reduction of Fe^{3+}, Fe^{2+} and Zn^{2+} to Fe^0 and Zn^0, as well as the formation of amorphous Li$_2$O, respectively [19,31,32]. The ZnFe$_2$O$_4$ sample obtained at 500 °C delivers the initial discharge and charge capacities of 1456 and 1074 mAh g^{-1}, respectively. While 1339 and 1112 mAh g^{-1} were obtained for ZnFe$_2$O$_4$ sample synthesized at 700 °C. The main reason for different initial charge–discharge capacities is that the sample obtained at low temperature has a higher surface area relative to high temperature. It is well known that the electrodes with higher surface area may lead to more side reactions with the

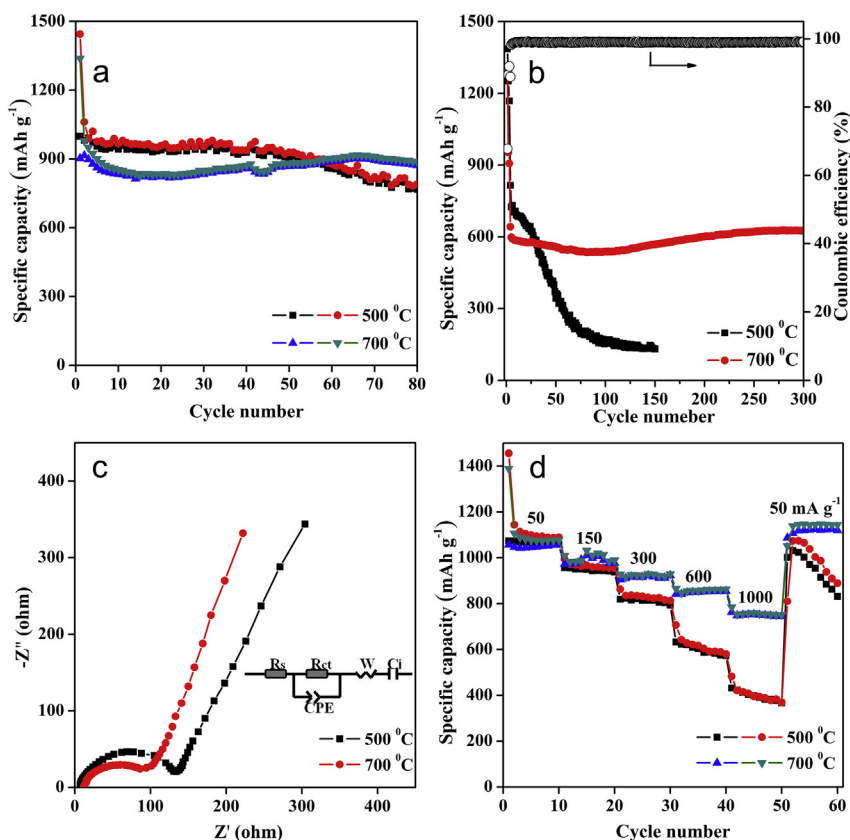**Fig. 5.** Cycling performance and plots of coulombic efficiency vs. cycle number for ZnFe$_2$O$_4$ obtained at 500 °C and 700 °C at a current density of (a) 150 mA g^{-1} and (b) 1000 mA g^{-1} (0.01–3.0 V). (c) Rate performance of ZnFe$_2$O$_4$ obtained at 500 and 700 °C. (d) Nyquist plots of Li/ZnFe$_2$O$_4$ cells charged to 2.8 V, inset of (d) shows the equivalent circuit.

electrolytes to form the solid electrolyte interphase, and give a higher first discharge capacity [3,33]. But, more side reactions may lead to lower coulombic efficiency [3,33]. Hence, the coulombic efficiency for the first cycle of $ZnFe_2O_4$ obtained at 500 °C is 74%, which is lower than that of $ZnFe_2O_4$ obtained at 700 °C (83%).

Since the temperature has a great effect on the cycling performance of the electrodes [26,28,29], the electrochemical performances of $ZnFe_2O_4$ nanorods obtained at different temperatures were further investigated between 0.01 and 3 V (vs. Li/Li$^+$). As presented in Fig. 5a, $ZnFe_2O_4$ obtained at 500 °C shows a slightly higher specific capacity at a rate of 150 mA g^{-1} than that of $ZnFe_2O_4$ obtained at 700 °C before 50 cycles. But this order is reversed after 80 cycles. $ZnFe_2O_4$ obtained at 500 °C delivers a specific capacity of 790 mAh g^{-1}, lower than 888 mAh g^{-1} from $ZnFe_2O_4$ obtained at 700 °C. The similar case also happens to the high rates. At a current density of 1000 mA g^{-1}, the specific capacity of $ZnFe_2O_4$ obtained at 500 °C is still higher than that of the sample obtained at 700 °C at the beginning of the cycling test (Fig. 5b). After 35 cycles, the specific capacity of $ZnFe_2O_4$ obtained at 500 °C, quickly drops to 200 mAh g^{-1}. That of $ZnFe_2O_4$ obtained at 700 °C could be maintained to 625 mAh g^{-1} even after 300 cycles. The above results indicate that the $ZnFe_2O_4$ synthesized at 500 °C shows a higher initial capacity but with worse retention. This phenomenon maybe caused by a large surface area which offers better contacting between the electrode and electrolyte and benefits the lithium storage during the lithiation/delithiation processes. On the other hand, larger surface area also probably increases the unwanted side reactions on the surface like the formation of a solid electrolyte interface (SEI) layer and then causes a rapidly decay of the specific capacity [33]. In addition, $ZnFe_2O_4$ nanorods obtained at 700 °C

with the improvement of crystallinity which may also contribute to better cycling performance [21,28,29]. Furthermore, in order to reveal the transport kinetics for the electrochemical properties of $ZnFe_2O_4$ nanorods obtained at different temperatures, electrochemical impedance spectroscopy (EIS) measurements were carried out after 30 cycles at the current density of 1000 mA g^{-1}. As shown in Fig. 5c, the impedance spectra consisted of one depressed semicircles in the middle frequency region is related to the charge transfer resistances R_{ct} [20,32]. And the charge transfer resistances of $ZnFe_2O_4$ obtained at 700 °C is 95 Ω, which is lower than that of $ZnFe_2O_4$ obtained at 500 °C (140 Ω) after cycling 30 cycles at the current density of 1000 mA g^{-1}. It may state that the sample obtained at high temperature may favor the electronic transmission and lead to a small internal resistance as well as good capacity retention.

Additionally, the capacity of $ZnFe_2O_4$ nanorods obtained at 700 °C is higher than most of the previous works, such as Ag-doped $ZnFe_2O_4$ thin films (434 mAh g^{-1} over 100 cycle) [30], $ZnFe_2O_4$/C hollow spheres (625 mAh g^{-1} cycling up to 30 cycles at 500 mA g^{-1}) [32], $ZnFe_2O_4$ nanoparticle (833.6 mAh g^{-1} cycling up to 50 cycles at 116 mA g^{-1}) [31] and so on. This could be attributed to $ZnFe_2O_4$ nanorods with special 1D nanostructure which may allow for efficient electrode−electrolyte contact and effective 1D electron transfer pathways. Importantly, as shown in Fig. S3, the 1D morphology of $ZnFe_2O_4$ was basically kept after 50 cycles at 1000 mA g^{-1}, revealing its structural and dimensional stability of the nanorods.

Apart from the high specific capacity and good cyclability, the rate capability is another very important property for high performance LIBs. Fig. 5d shows the rate performance of $ZnFe_2O_4$ samples
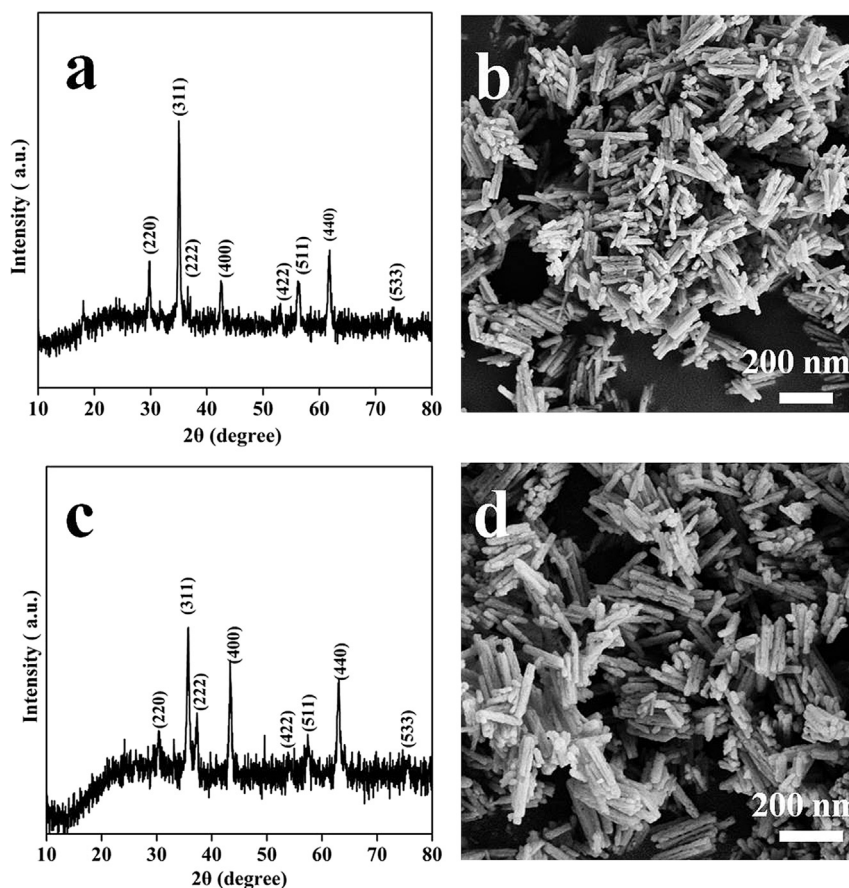

Fig. 6. XRD patterns of (a) $CoFe_2O_4$ nanorods, (b) $NiFe_2O_4$ nanorods, the SEM images of (c) $CoFe_2O_4$ nanorods, (d) $NiFe_2O_4$ nanorods.

at different current densities between 3.0 and 0.01 V, it can be seen that ZnFe$_2$O$_4$ nanorods (700 °C) exhibits the average discharge capacity of 1040, 970, 900, 850, 750 mAh g^{-1} at the current densities of 50, 150, 300, 600, and 1000 mA g^{-1}, respectively. The other significant result is the restoration of the ZnFe$_2$O$_4$ after high rate cycling. When the current density restores to 50 mA g^{-1} after 10 cycles at 1000 mA g^{-1}, the cell recovers full charge capacity of 1050 mAh g^{-1}, indicating the stability of the anodes in a wide range of current densities. For comparison, ZnFe$_2$O$_4$ obtained at 500 °C shows the average discharge capacity of 1120, 960, 830, 605 and 395 mAh g^{-1} at the corresponding current densities of 50, 150, 300, 600, and 1000 mA g^{-1}, respectively. Furthermore, the higher current density, the more severe capacity decay of ZnFe$_2$O$_4$ obtained at 500 °C is observed, while the ZnFe$_2$O$_4$ nanorods obtained at 700 °C shows very stable capacity at varied current densities. The advantages of this nanostructure as well as its high capacity make ZnFe$_2$O$_4$ nanorods obtained at 700 °C a very promising candidate as an anode material for the rechargeable lithium ion batteries.

3.2. CoFe$_2$O$_4$ and NiFe$_2$O$_4$ nanorods

Substituting Zn by Co or Ni in the ferrite stoichiometry, the XRD patterns and the TEM images show that the synthesized samples at 700 °C are CoFe$_2$O$_4$ (JCPDS Card, No. 22-1086) and NiFe$_2$O$_4$ (JCPDS Card, No. 10-0325) nanorods, respectively (Fig. 6), which are similar to ZnFe$_2$O$_4$. This result indicates that this method is an effective, simple and general way to prepare 1D spinel Fe-based binary transition metal oxide materials. And the electrochemical

properties of the synthesized samples (CoFe$_2$O$_4$ and NiFe$_2$O$_4$) were also studied.

Fig. 7 shows the electrochemical properties of CoFe$_2$O$_4$ and NiFe$_2$O$_4$ nanorods. CoFe$_2$O$_4$ delivers the first discharge and charge capacities of 1694 and 1298 mAh g^{-1} (Fig. 7a) with a coulombic efficiency of 74.8%. The reversible capacity of CoFe$_2$O$_4$ retains at approximately 800 mAh g^{-1} at the current density of 1000 mA g^{-1} even after 300 cycles (coulombic efficiency about 99%). This result is superior to that of CoFe$_2$O$_4$/graphene nanocomposite (565 mAh g^{-1} after 300 cycles at current density 800 mA g^{-1}) [34], macroporous CoFe$_2$O$_4$ (initial specific capacity of 1782 mAh g^{-1}, but with relatively poor capacity retention) [22]. The good performance may be attributed to the 1D structure of CoFe$_2$O$_4$ which can shorten Li$^+$ diffusion and relax large volume change. The CoFe$_2$O$_4$ nanorods electrode delivers the specific capacities of 1280, 1220, 1130, 960 and 840 mAh g^{-1} at the current densities of 50, 150, 300, 600, and 1000 mA g^{-1}, respectively. When back to low current density, the capacity of the electrode can return to the corresponding initial value implying that the electrode is stable at different current densities. Compared to the previous reports about CoFe$_2$O$_4$, the rate capacity and cycling stability of the CoFe$_2$O$_4$ are improved [22,34].

As for NiFe$_2$O$_4$, few reports are available on electrochemical lithium storage properties of its nanostructures. Macroporous NiFe$_2$O$_4$ was synthesized through a sol–gel method which delivered a capacity of 600 mAh g^{-1} after 80 cycles at the rate of 1C, but it was lack of long term cycling performance [21]. NiFe$_2$O$_4$ nanocrystalline was prepared by anodization of the alloy films at room temperature and exhibited a low reversible capacity of 355 mAh g^{-1} [35]. NiFe$_2$O$_4$ nanorods in our work delivers the first discharge and charge
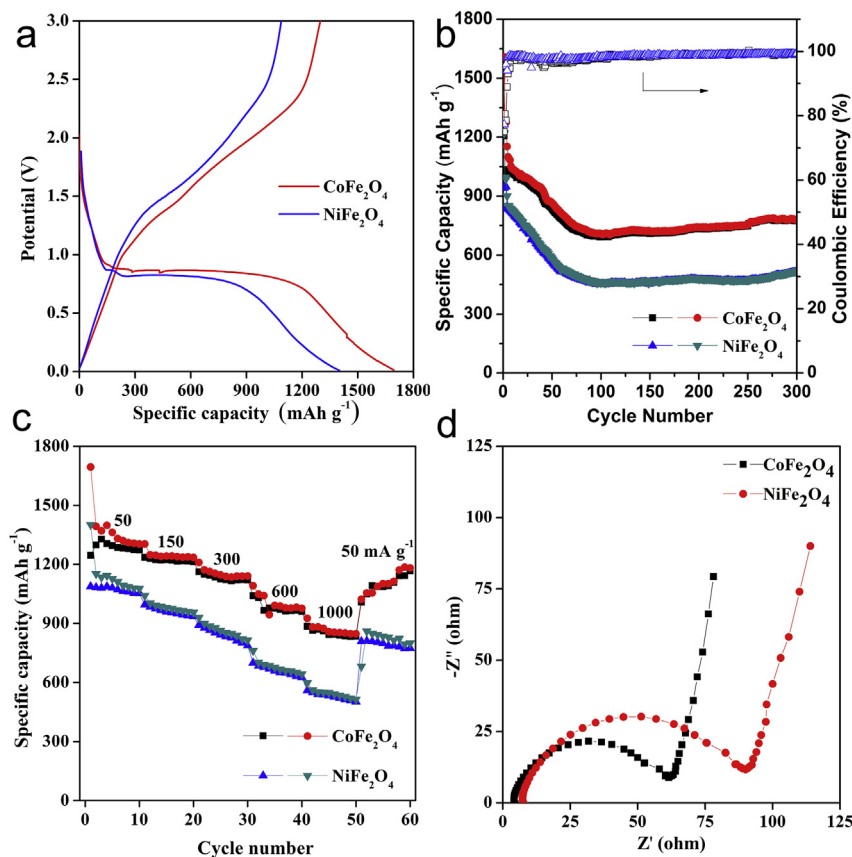

Fig. 7. (a) The initial charge–discharge profiles of the CoFe$_2$O$_4$ and NiFe$_2$O$_4$ nanorods at a current density of 150 mA g^{-1} in the voltage range 0.01–3.0 V. (b) Plot of capacity and coulombic efficiency vs. cycle number for CoFe$_2$O$_4$ and NiFe$_2$O$_4$ (0.01–3.0 V, 1000 mA g^{-1}), (c) rate performance of CoFe$_2$O$_4$ and NiFe$_2$O$_4$. (d) Nyquist plots of Li/CoFe$_2$O$_4$ cells and Li/NiFe$_2$O$_4$ charged to 2.8 V after 1st cycle (0.01–3.0 V, 150 mA g^{-1}).

capacities of 1401 and 1087 mAh g^{-1}, with a coulombic efficiency of 77.5% (Fig. 7a). The reversible capacity of NiFe$_2$O$_4$ nanorods is 520 mAh g^{-1} at the current density of 1000 mA g^{-1} after 300 cycles (Fig. 7b), while this long-term cycling (up to 300 cycles at 1000 mAh g^{-1}) performance has not been reported yet [21,35]. For the rate capability of NiFe$_2$O$_4$ nanorods, its capacity loss along with the increasing current density is more serious than that of CoFe$_2$O$_4$ nanorods (Fig. 7c). This can be ascribed to the larger charge transfer resistance (R_{ct}) of NiFe$_2$O$_4$ nanorods (90 Ω) compared to that of CoFe$_2$O$_4$ (60 Ω) as presented in Fig. 7d. In addition, as shown in Fig. S4, the electrochemical properties of CoFe$_2$O$_4$ and NiFe$_2$O$_4$ prepared at 500 °C are also inferior to those obtained at 700 °C. The above results indicate that MFe$_2$O$_4$ (M = Zn, Co, Ni) nanorods (700 °C) are promising anode candidates for the LIBs.

4. Conclusion

In conclusion, MFe$_2$O$_4$ (M = Zn, Co, Ni) nanorods were successfully synthesized using a template-engaged reaction with β-FeOOH nanorods and their corresponding acetates at 700 °C for 2 h in air. The reversible capacity of 800, 625 and 520 mAh g^{-1} were obtained for CoFe$_2$O$_4$, ZnFe$_2$O$_4$ and NiFe$_2$O$_4$, respectively, at the high current density of 1000 mA g^{-1} even after 300 cycles. The merits of this nanostructure and its high reversible capacity make MFe$_2$O$_4$ (M = Zn, Co, Ni) nanorods very prospective candidates as anode materials for rechargeable lithium ion batteries. We also discovered that the reaction temperatures have great impact on the electrochemical properties of MFe$_2$O$_4$ nanorods.

Acknowledgments

Appendix A. Supplementary data

Supplementary data related to this article can be found at http://dx.doi.org/10.1016/j.jpowsour.2013.08.109.

References

[1] M. Armand, J.M. Tarascon, Nature 451 (2008) 652–657.
[2] J.M. Tarascon, M. Armand, Nature 414 (2001) 359–367.
[3] P.G. Bruce, B. Scrosati, J.M. Tarascon, Angew. Chem. Int. Ed. 47 (2008) 2930–2946.
[4] M.R. Palacn, Chem. Soc. Rev. 38 (2009) 2565–2575.
[5] Y. Idota, T. Kubota, A. Matsufuji, Y. Maekawa, T. Miyasaka, Science 276 (1997) 1395–1397.
[6] H.E. Wang, Z.G. Lu, D. Qian, Y.J. Li, W. Zhang, Nanotechnology 18 (2007) 115616.
[7] Y.M. Lin, P.R. Abel, A. Heller, C.B. Mullins, J. Phys. Chem. Lett. 2 (2011) 2885–2891.
[8] Z.C. Bai, N. Fan, C.H. Sun, Z.C. Ju, C.L. Guo, J. Yang, Y.T. Qian, Nanoscale 5 (2013) 2442–2447.
[9] H.B. Wu, J.S. Chen, H.H. Hng, X.W. Lou, Nanoscale 4 (2012) 2526–2542.
[10] M.S. Whittingham, Dalton Trans. 40 (2008) 5424–5431.
[11] Y.S. Lin, J.G. Duh, M.H. Hung, J. Phys. Chem. C 114 (2010) 13136–13141.
[12] Y.G. Wang, H.Q. Li, P. He, E. Hosono, H.S. Zhou, Nanoscale 2 (2010) 1294–1305.
[13] H.B. Wang, Q.M. Pan, Y.X. Cheng, J.W. Zhao, G.P. Yin, Electrochim. Acta 54 (2009) 2851–2855.
[14] F.Y. Cheng, J. Liang, Z.L. Tao, J. Chen, Adv. Mater. 23 (2011) 1695–1715.
[15] A.S. Arico, P. Bruce, B. Scrosati, J.M. Tarascon, W. VanSchalkwijk, Nat. Mater. 4 (2005) 366–377.
[16] Y. Wang, G.Z. Cao, Adv. Mater. 20 (2008) 2251–2269.
[17] P. Poizot, S. Laruelle, S. Grugeon, L. Dupont, J.M. Tarascon, Nature 407 (2000) 496–499.
[18] X.W. Guo, X. Lu, X.P. Fang, Y. Mao, Z.X. Wang, L.Q. Chen, X.X. Xu, H. Yang, Y.N. Liu, Electrochem. Commun. 12 (2010) 847–850.
[19] Z. Xing, Z.C. Ju, J. Yang, H.Y. Xu, Y.T. Qian, Nano Res. 5 (2012) 477–485.
[20] P.F. Teh, Y. Sharma, S.S. Pramana, M. Srinivasan, J. Mater. Chem. 21 (2011) 14999–15008.
[21] P. Lavela, J.L. Tirado, J. Power Sources 172 (2007) 379–387.
[22] Z.H. Li, T.P. Zhao, X.Y. Zhan, D.S. Gao, Q.Z. Xiao, G.T. Lei, Electrochim. Acta 55 (2010) 4594–4598.
[23] Y. Wang, D.W. Su, A. Ung, J.H. Ahn, G.X. Wang, Nanotechnology 23 (2012) 055402.
[24] H.X. Zhao, Z. Zheng, K.W. Wong, S.M. Wang, B.J. Huang, D.P. Li, Electrochem. Commun. 9 (2007) 2606–2610.
[25] Y.L. Ding, J. Xie, G.S. Cao, T.J. Zhu, H.M. Yu, X.B. Zhao, Adv. Funct. Mater. 21 (2011) 348–355.
[26] N. Yan, L. Hu, Y. Li, Y. Wang, H. Zhong, X.Y. Hu, X.K. Kong, Q.W. Chen, J. Phys. Chem. C 116 (2012) 7227–7235.
[27] Y.F. Deng, Z.E. Li, Z.C. Shi, H. Xu, F. Peng, G.H. Chen, RSC Adv. 2 (2012) 4645–4647.
[28] Y. Ding, Y.F. Yang, H.X. Shao, Solid State Ionics 217 (2012) 27–33.
[29] S.W. Oh, H.J. Bang, Y.C. Bae, Y.K. Sun, J. Power Sources 173 (2007) 502–509.
[30] Y.N. NuLi, Y.Q. Chu, Q.Z. Qin, J. Electrochem. Soc. 151 (2004) A1077–A1083.
[31] Y. Ding, Y.F. Yang, H.X. Shao, Electrochim. Acta 56 (2011) 9433–9438.
[32] Y.F. Deng, Q.M. Zhang, S.D. Tang, L.T. Zhang, S.N. Deng, Z.C. Shi, G.H. Chen, Chem. Commun. 47 (2011) 6828–6830.
[33] A. Vu, Y.Q. Qian, A. Stein, Adv. Energy Mater. 9 (2012) 1056–1085.
[34] S.Y. Liu, J. Xie, C.C. Fang, G.S. Cao, T.J. Zhu, X.B. Zhao, J. Mater. Chem. 22 (2012) 19738–19743.
[35] Y.N. NuLi, Q.Z. Qin, J. Power Sources 142 (2005) 292–297.